Hindawi
Advances in Tribology
Volume 2020, Article ID 3761745, 18 pages
https://doi.org/10.1155/2020/3761745

Research Article

Effect of Load on the Tribological Properties of Eutectic Al-Si Reinforced n-Al_2O_3 under Dry Sliding Conditions

Pranav Dev Srivyas and M.S. Charoo

Mechanical Engineering Department, National Institute of Technology, Srinagar, India

Correspondence should be addressed to Pranav Dev Srivyas; devpranav.srivyas_17@nitsri.net

Received 5 October 2019; Accepted 17 December 2019; Published 7 February 2020

Academic Editor: Patrick De Baets

Advanced composites are the materials of the new generation. Hence, the focus of the study is to determine the tribological properties of the eutectic Al-Si alloy reinforced with (2, 4, 6, 8, and10 wt. %) of n-Al_2O_3 against chrome-plated steel ball under dry sliding conditions. The novelty of this work is the fabrication of the composite sample with this elemental composition, which is not done before. Spark plasma sintering (SPS) nonconventional fabrication method is used to fabricate advanced composite samples. Friction coefficient (COF) and wear rate of the composite samples were studied under high load, varying from 50 N to 300 N, using the ball-on-disc tribometer configuration, with other parameters such as stroke, frequency, sliding distance, and sliding velocity remaining constant at 2 mm, 30 Hz, 120 meter, and 0.120 m/s, respectively. Reduction in wear volume for the advanced composite was reported in the range 15.45–44.58% compared to the base alloy (eutectic Al-Si alloy). An increase in friction coefficient was reported in the range 28.80–35.65% compared to the base matrix alloy material. It was also reported that the wear rate increases and the friction coefficient of the composite sample decreases with an increase in load for the tribo-pair. It was observed that an increase in the wt. % of reinforcement influences the friction and wear behavior of the composite. Wear mechanism at high load was characterized by plastic deformation, adhesion, delamination, and abrasion wear. For pre- and postcharacterization of surface and worn tracks, scanning electron microscopy (SEM) electron dispersion spectroscopy (EDS), 3D surface profilometer, and optical microscopy were used. This work aimed to investigate the influence of load on the tribological properties of Al-Si eutectic reinforced n-Al_2O_3 under dry sliding conditions. Its main objective was to provide a new contribution to the tribological behavior of these composites fabricated using the nonconventional spark plasma sintering method.

1. Introduction

Wear is the removal of material from one or both surfaces, or surface damage when one or both surfaces are in a sliding or rolling motion, or in an impact motion relative to other surface. Wear is the prominent problem that causes continuous loss of material and further leads to a 1–4% increase in cost due to the low efficiency of the material and reduces the actual life of the material and its components in various engineering applications [1]. Serious efforts have been made to reduce the wear of materials and to increase the life of the components, and thereby improve the durability of the materials. To improve the durability and modify the bulk properties of the materials, certain modifications such as surface treatment process, inclusion of reinforcements in the matrix material, and applications of coatings were used on the materials. Aluminum and its alloys are extensively used in industries nowadays [2]. Among all the commercially known aluminum alloys, Al-Si alloys show attractive mechanical and tribological properties, such as high strength to weight ratio, good wear obstruction, low thermal expansion coefficient, good thermal conductivity, and corrosion resistance. Al-Si binary alloy has found wide applications in the automotive industry (IC engine components), the aerospace industry, high-speed rotating machinery in marine applications, etc. [3–5]. The performance properties of the Al-Si binary alloy depend on its microstructure. The microstructure consists of Al as the primary phase in the hypereutectic and Si as the primary phase in the eutectic and hypoeutectic Al-Si alloy. During solidification, grain

refinement takes place, which leads to improved mechanical and tribological properties of the Al-Si binary alloy [6, 7]. Due to their extensive properties, these alloys are used as a substitute for cast iron in the automotive industry. Replacing cast iron with aluminum alloy for IC engine application has the potential for a sizable reduction up to 45% for the gasoline engine. It is also reported by the analysis that most of the IC engine components fail due to wear loss (~25–45%) and friction loss (~45%). A number of previous researches have been reported on the wear of Al-Si alloys. Shivanath et al. [8] reported that an increase in the silicon content in the alloy increases the wear resistance of the alloy up to the eutectic composition. Bai and Biswas [9] reported that no structural trends have been recognized with an increase in the Si content with respect to the wear rate. Eyre [10] reported that the etched surface of the Al-Si binary alloy produced reduced wear and friction. It was explained that this reduced wear and COF might be due to the layer of the etched material between the alloy and the counter-face which reduces direct metal-metal contact. Clegg and Das [11] studied the effect of structural modification on the wear resistance of the hypereutectic Al-Si alloy.

Experimental studies were conducted on a pin-on-disc tribometer with different load and sliding distance conditions, and it was reported that structural modifications do not have much effect on the wear resistance of the alloy. In another research, the wear behavior of the eutectic Al-Si alloy and heat-treated Al-Si alloy was studied, and it was reported that an increase in the sliding speed of the disc leads to an increase in the wear loss. It was also reported that the wear rate of the heat-treated Al-Si alloy is less than that of the eutectic Al-Si alloy sample, and it was explained that heat treatment might affect the hardness of the sample and, hence, the wear resistance. Rajaram et al. [12] studied the tensile and wear properties of an Al-Si alloy. It was reported that an oxide film was found, which helped reduce direct metal-metal contact and, hence, the abrasive wear of the alloy. Dhiman et al. [13] studied the wear analysis of a multicomponent cast alloy (Al-17Si-0.8Ni-0.6Mg-1.2Cu-0.6Fe) and reported that the wear rate reduced at high sliding speed, which might be due to the oxide layer formation on the sliding interface. Whereas several studies [14] were based on the tribological behavior of the Al-Si alloy, only few studies were made on the tribological behavior of eutectic Al-Si reinforced with hard ceramic. Srivyas and Charoo [15] studied the tribological behavior of a hybrid self-lubricating composite at high applied load (100 N–300 N). From the study, it was observed that addition of ceramic and graphene self-lubricating particles in the Al-Si eutectic alloy improves the tribological and mechanical properties of the fabricated composite. In this present study, the focus is toward the traditional characterization of the eutectic Al-Si alloy as a matrix material reinforced with n-Al_2O_3 with varying content (2 wt. %–10 wt. %) fabricated using the nonconventional spark plasma sintering method. The tribological studies were made at high load to examine the properties of the composite against a chrome-plated steel ball in dry sliding conditions.

2. Material Selection and Sample Fabrication

Pre-alloyed aluminum-silicon (Al-Si) eutectic alloy powder (procured from Intelligent Materials Pvt. Ltd., India) with an average particle size (APS) of 60–70 μm was used as the matrix material for the composite (Figure 1). The chemical composition of the matrix alloy aluminum powder is Si ~10.244%, Fe < 0.8%, Cu < 0.3%, Zn < 0.2%, Mn < 0.15, Mg < 0.1%, and Al balance (purity 99.99%). Nano-γ-Al_2O_3 (Figure 2) of size 20 nm with purity 99.99% was used as the reinforcement in the matrix aluminum alloy with different weight percentages (2, 4, 6, 8, and 10 wt. %). Theoretical density of the eutectic Al-Si alloy and nano-γ-Al_2O_3 is 2.66 g/cm^3 and 3.95 g/cm^3, respectively. Matrix Al-Si-based alloy powder was then ball milled in a high-energy planetary ball mill (FRITSCH GmbH, PULVERISETTE 5/4 CLASSIC LINE) with nano-γ-Al_2O_3 reinforcement to produce a homogeneous mixture. For the milling procedure, the powder was loaded into a silicon nitride jar. Wet mixing was done in ethanol medium, which was used as the "process controller agent" to prevent cold weld of the powder with the jar walls. Silicon nitride balls of 10 mm diameter were used for the blending purpose with a weight ratio of ball to powder of 10 : 1. Milling was performed at 240 rpm for 12 hours with a periodic halt of 15 minutes after every 2 hours of milling so as to maintain the milling temperature and to prevent accumulation of the powder on the walls of the jar. The milling was done with different wt. % (i.e., 2, 4, 6, 8, and 10 wt. %) of the reinforcement in the matrix alloy. After the milling process, the suspension of matrix-reinforcement in ethanol was dried in a vacuum evaporator at 50°C temperature for 3 hours followed by heating in a vacuum oven at the constant temperature of 50°C for 60 minutes to completely remove the moisture content. To prevent oxidation of the powder composition, the milled powder was kept in the glove box to minimize contamination and oxidation of the composite powder samples.

After milling of the powder with different wt. % concentrations, fabrication was done using the SPS nonconventional fabrication and consolidation method. By using SPS fabrication method (Dr. Sinter-SPS-625, Fuji-Electronic INDUSTRIAL Co. Ltd. Japan), a maximum temperature of up to 2400°C can be achieved to fabricate the sample by using a standard graphite die of diameter 30 mm (Figure 3). Fabrication of all samples (from base composition to maximum wt. % reinforcement sample) was done at 450°C sintering temperature and a heating rate of 100°C/min; a constant pressure of 50 MPa and a holding time of 10 minutes under argon atmosphere were used throughout the whole process (Figure 4). As the powder started to sinter, current flowed through the graphite die. Control of the sintering temperature is possible by setting the ramp rate, pulse current, holding time, pulse duration, and voltage. The whole process of fabrication was done in four steps: (1) removal of gages from the chamber and vacuum creation by DC pulse current flow, (2) application of pressure, (3) resistance heating, and (4) cooling. When pressure is applied on the die, the current passes through the sample and heats the powder rapidly. The sintering is done in a controlled

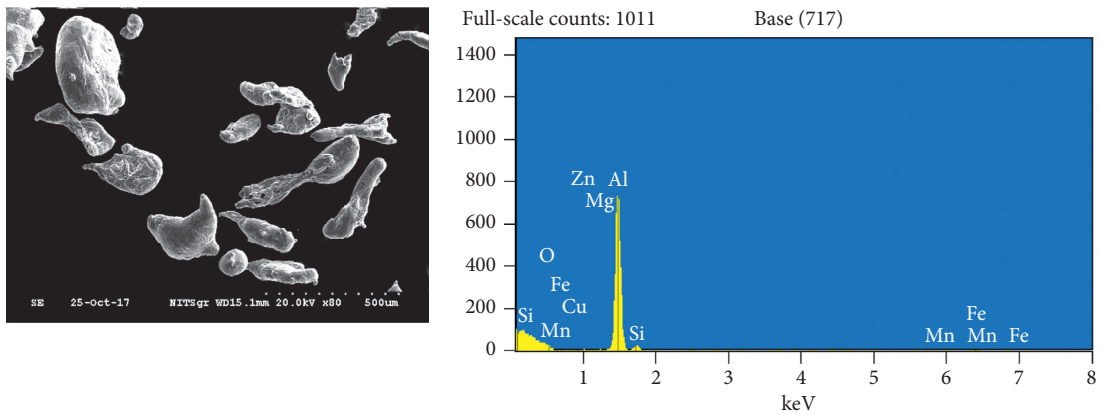

Figure 1: SEM and EDS of eutectic Al-Si alloy powder.

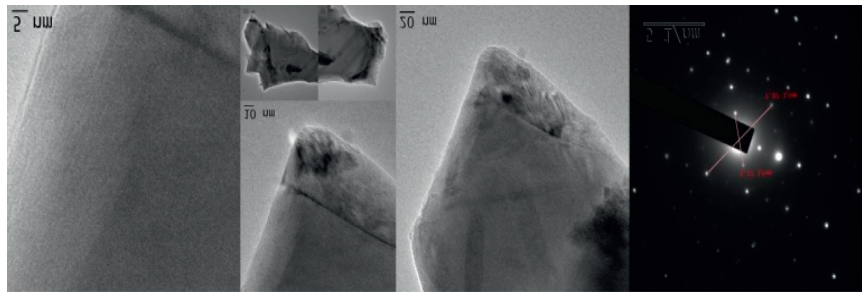

Figure 2: TEM images of the eutectic Al-Si alloy and nano-Al_2O_3 powder.

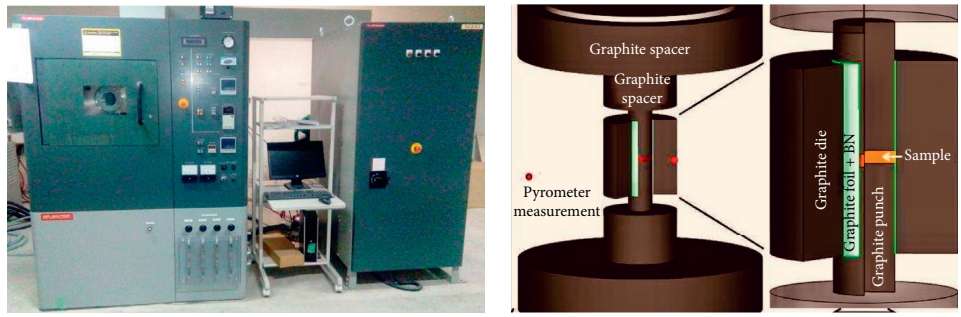

Figure 3: (a) Spark plasma sintering machine. (b) Spark plasma sintering (schematic).

atmosphere, which enables controlled reduction and leads to the fabrication of fully dense samples. This process does not require any binder and precompaction as the consolidation and sintering go hand in hand. Clear grain boundaries, increase in plasticity, improved interfacial bonding, and segregation of reduced impurities are key advantages of this fabrication method. The whole process of sample fabrication takes 14 minutes 30 seconds. The sintered samples are then removed from the die after rapid cooling. The fabricated sample has the dimension of thickness 10 mm and diameter 30 mm. The sintered samples are then polished by grinding on an automatic sample polishing machine using SiC emery paper with (220–2000) grit size. The samples are then polished using diamond paste (5 μm–0.25 μm) and an aerosol spray on a velvet paper to obtain a mirror-polished surface. The theoretical density of base aluminum alloy is 2.66 g/cm^3 and of nano-alumina is 3.95 g/cm^3, which were used to obtain the mixture density, δ_m, calculated using the rule of mixture:

$$\delta_m = \frac{W_{al} + W_{alu}}{(W_{al}/\rho_{al}) + (W_{alu}/\rho_{alu})}, \quad (1)$$

where δ_m is the theoretical density of the mixture, W_{al} is the weight percentage of aluminum alloy powder, W_{alu} is the weight percentage of nano-alumina powder, ρ_{al} is the

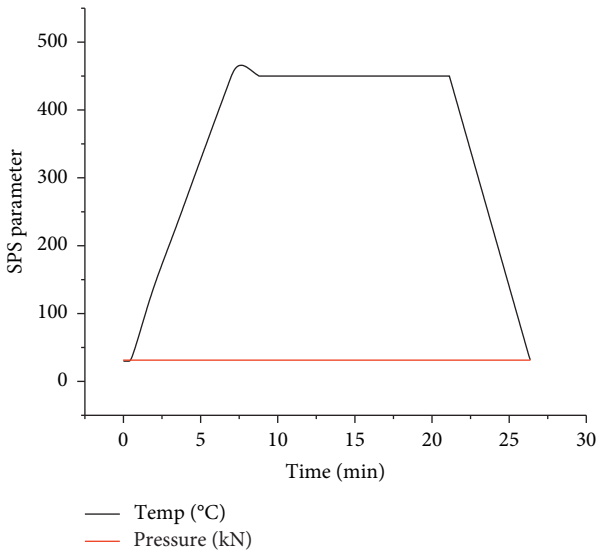

Figure 4: SPS parameter variation with time.

specific weight of the base aluminum alloy, and ρ_{alu} is the specific weight of nano-alumina powder.

Based on (1), the density of the nano-reinforced aluminum matrix composites was expected to increase, as the specific weight of the reinforcements seems to be more than that of the aluminum alloy. The theoretical values and practical values of the reinforced composites are presented in Table 1 (Figure 5). The bulk density/practical density (ρ_p) of the sintered sample was measured using a digital densimeter based on the Archimedes principle (based on (2)). Highly dense and compact samples were obtained using the SPS fabrication method at low temperature:

$$\rho_p = \frac{W_{air}}{W_{air} - W_{water}} \times \rho_w, \tag{2}$$

where ρ_p is the bulk density/practical density after sintering, W_{air} is the weight of the sample in air, W_{water} is the weight of the sample in water, and ρ_w is the density of the distilled water, i.e., 1 g/cm^3.

Porosity volume percentage of the sintered sample was calculated according to the following equation:

$$\text{porosity (\%)} = 100 - \frac{\text{sintered density}}{\text{theoretical density}} \times 100. \tag{3}$$

3. Experimental Procedure

3.1. Hardness Studies. Micro-Vicker hardness tests were carried out to determine the hardness value of the base alloy samples and composite samples. A digital microhardness tester (HVD-1000 MP) was used in this study for testing the hardness (Figure 6). Hardness tests were performed thrice on each spark plasma sintered sample to determine their hardness values. In micro-Vicker hardness studies, the composite specimens were compressed with a diamond indenter at a certain load for a certain staying time. After load removal, the diagonal indents were analyzed using an optical microscope to determine the Vicker hardness number. The ratio between the area of residual impression and indentation load helps to determine the hardness number. Microhardness of a material has a significant influence on the material's wear properties.

3.2. Tribological Test Procedure. Tribo test was conducted on a ball-on-disc; Figure 7(b) shows a universal tribometer and Figure 7(a) shows the reciprocating configuration under dry conditions. The tribometer is computer controlled with data acquisition systems and sensors installed in the tribo setup and in the computer system, respectively. The composite disc was made to oscillate on the lower drive with linear displacement. The holder with the counter ball remains stationary at its mean position over the disc sample with contact applied load. In this experimental study, the effect of high load on the tribological behavior of the composite was studied. Tribo-load tests were conducted with load differences from 50 N to 300 N, with other parameters such as stroke, frequency, sliding distance, and sliding velocity remaining constant at 2 mm, 30 Hz, 120 m, and 0.120 m/s, respectively. The sample and counter ball are properly cleaned and dried before and after the tests. COF is measured by using the data acquisition system installed in the computer system. Here, the wear volume (mm^3) is measured using a 3D surface profilometer, and the wear rate is measured by using

$$\text{wear rate} = \frac{\text{wear volume}}{\text{sliding distance} \times \text{load}}. \tag{4}$$

3.3. Tribological Characterization. Different characterization techniques are used to examine the microstructural matrix and wear surface after and before testing. These characterization techniques include optical microscopy on Leica DM-6000 M. SEM and EDS studies were conducted using HITACHI S3600 N. Profilometer studies were performed using an R-tech 3D surface profilometer (USA), which analyzes surface roughness of the polished surface, and wear scar, and calculates wear volume as well.

3.4. Microstructural Studies. The surface of the fabricated sample was prepared by grinding and polishing the composite sample using emery paper, followed by diamond paste and aerosol spray on velvet cloth to obtain a mirror-polished surface of the sample, which is further subjected to various microstructural studies. Optical microscopy at low and high magnification was done on all the composite samples. Figure 8 presents the optical images of the samples. Uniform distribution of the reinforcements in the matrix was almost achieved, but in some spots, there is clustering of nano-reinforcement particles with increasing particle percentage. The dark black region indicates the presence of Al_2O_3 in the composite. So, optical micrographs revealed the presence of clustering/agglomeration for certain percentage of the reinforcement samples, which might lead to segregation of the particles, and porosity, which indeed affects the practical density of the samples.

Table 1: Theoretical density, practical density, and porosity content comparison for different composition samples.

Composition	Reinforcement wt. %	Theoretical density (g/cm^3)	Practical density (g/cm^3)	Density (%)	Porosity content (vol. %)
Base composition	Al-Si	2.66	2.65	99.62	0.3759
Composition 1	Al-Si + 2 wt.% Al_2O_3	2.68	2.654	99.02	0.9701
Composition 2	Al-Si + 4 wt.% Al_2O_3	2.712	2.666	98.30	1.696
Composition 3	Al-Si + 6 wt.% Al_2O_3	2.737	2.691	98.31	1.680
Composition 4	Al-Si + 8 wt.% Al_2O_3	2.763	2.7	97.71	2.280
Composition 5	Al-Si + 10 wt.% Al_2O_3	2.789	2.51	89.99	10.003

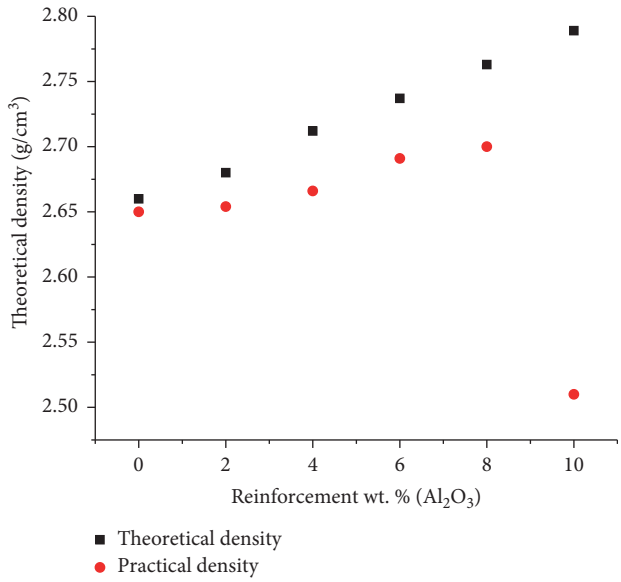

Figure 5: Density v/s reinforcement concentration.

Figure 6: HVD-1000 MP micro-Vicker hardness tester.

A smooth and clean interface was, thus, formed. Some clusters of the reinforcements were observed for high reinforcement particle percentage, at the nugget zone, which was observed by the SEM micrographs. An R-tech 3D surface profilometer was used to measure the surface roughness (Ra) of the polished sample surface. The Ra of the composite sample varies between 0.005 and 0.008 μm (Figure 9). Roughness reading of the counter-body ball is 0.04 μm. So, from the microstructural analysis, it was clear that the uniform distribution is almost achieved. Very less agglomerates/clusters are formed in the composite samples, and good surface roughness is achieved as it is reported that

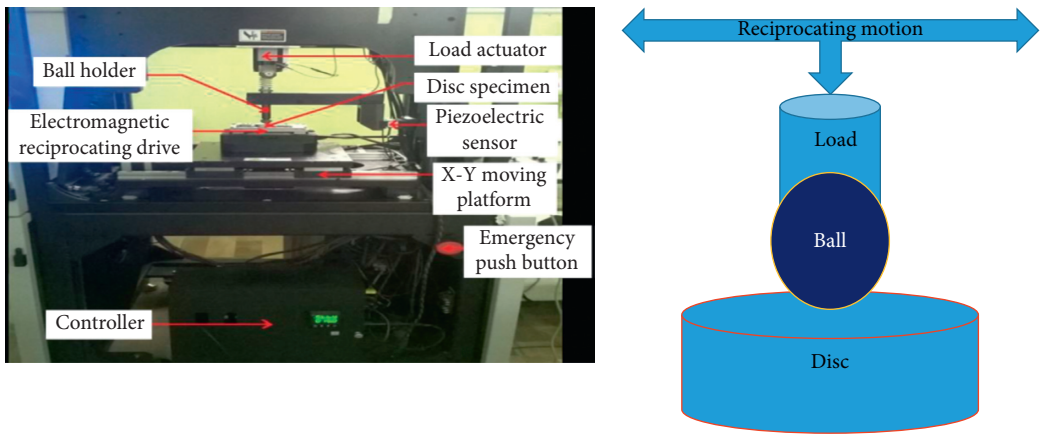

Figure 7: (a) Universal reciprocating ball-on-disc tribometer setup. (b) Schematic of the ball-on-disc reciprocating setup.

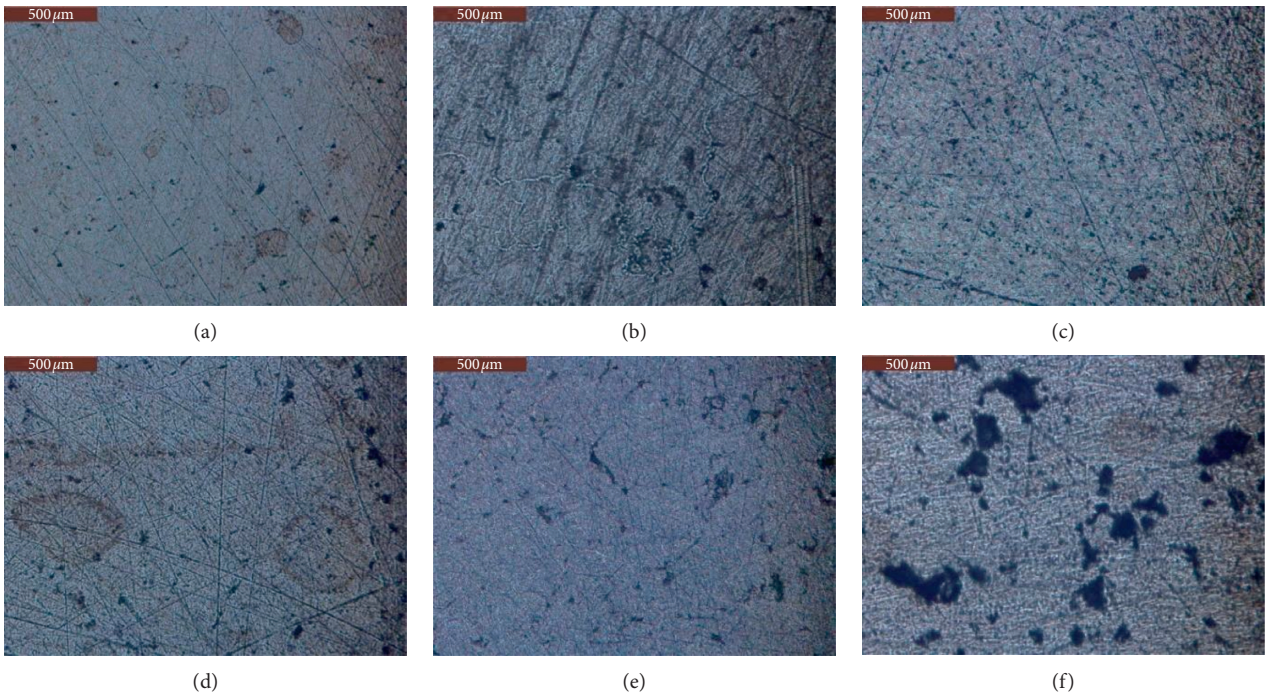

Figure 8: Optical micrographs of fabricated sample surface. (a) Base composition. (b) Composition 1. (c) Composition 2. (d) Composition 3. (e) Composition 4. (f) Composition 5.

the morphology and microstructural properties of the composite samples significantly influenced the mechanical and tribological properties of the samples.

4. Results and Analysis

4.1. Hardness. The effect of the reinforcement concentration applied in indentation load and the effect of dwell time were studied on all the fabricated specimens (Figure 10). The hardness test was carried out at varying loads (10gf, 25gf, 50gf, 100gf, 200gf, 300gf, and 500gf) with variable dwell time (1 sec, 5 sec, 10 sec, 15 sec, and 20 sec). For composition 3, maximum hardness values were achieved. Reinforcement concentration up to 6 wt. % increases the hardness properties of the composite specimens for variable loads and dwell time. However, after a certain time, a somewhat decrease in the hardness properties of the composite specimen was reported, which might be due to the clustering/agglomeration of reinforcement particles in the specimen. From the results, it was interpreted that the microhardness significantly depends on the reinforcement concentration and the applied load. With the increase in weight percentage of reinforcement, the hardness of the composite sample increases up to a certain limit. Dwell time affects the

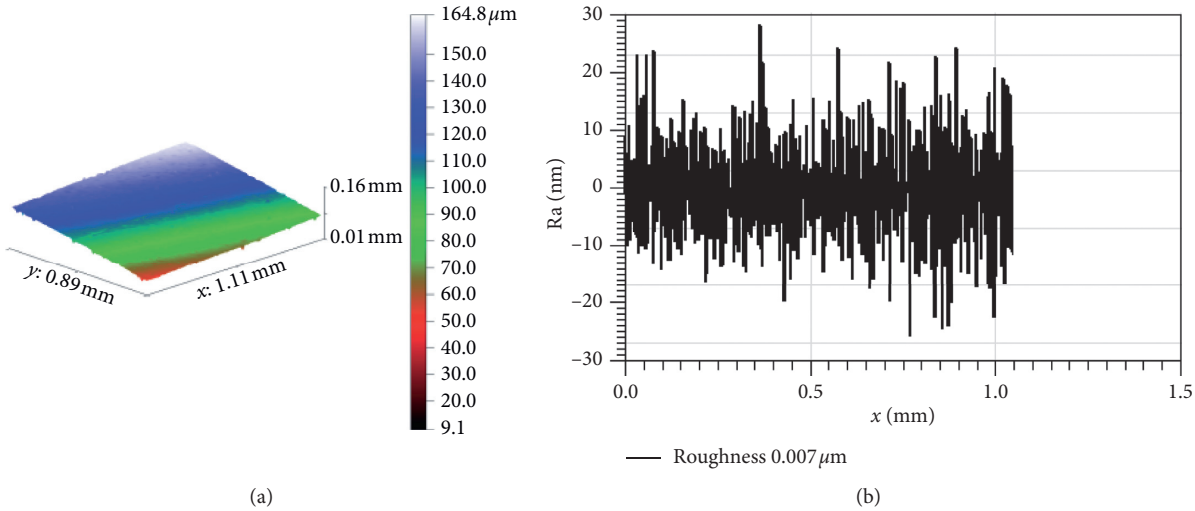

Figure 9: 3D surface profilometer analysis of the polished sample surface.

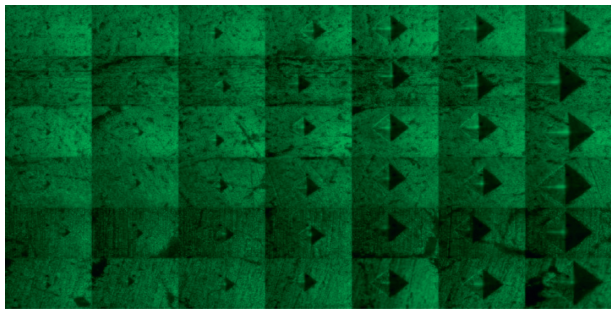

Figure 10: Micro-Vicker indentation on the composite samples.

hardness value of fabricated composite samples, but its effectuality was not much significant. Figure 11 shows the hardness value versus dwell time graph for different composition samples.

4.2. Friction and Wear Studies

4.2.1. Effect of Load and Reinforcement Concentration. Tribological friction and wear tests were conducted on all the composite specimens and base composition samples to study the effect of friction and wear behavior of fabricated samples, against the chrome-plated steel ball at room temperature. In this study, the load test with variable load of 50 N–300 N was performed on all samples with other parameters such as frequency, stroke, and sliding distance remaining constant in dry conditions. Each tribo-test was performed thrice for precision results. The results of the COF for variable loads for different compositions of samples obtained from the experimental studies are shown in Figure 12. COF versus normal applied load for base composition is shown in Figure 12(a). From the graph, the COF for the base composition against the chrome-plated steel ball under dry conditions decrease with an increase in applied load from 50 N to 250 N. The maximum (0.1216) and minimum (0.0814) COF values were observed for applied load of 50 N and 250 N, respectively. There was a continuous decrease in the COF of base composition from 50 N to 250 N load; at 300 N load, the value for COF again started to increase and is reported as 0.1202. For composition 1, the result is shown in Figure 12(b). A continuous decrease in the COF was reported for this composition specimen.

The minimum COF was obtained at 300 N load with a value of 0.0866, and maximum COF (0.1351) was reported at 50 N load. For composition 2, the value of COF increased up to 100 N load (0.1676) and then started to decrease. Minimum COF (0.984) was reported at 300 N load. The results for this composition are shown in Figure 12(c). Composition 3 showed a similar kind of result patterns as composition 2. From the graph in Figure 12(d), maximum (0.1554) and minimum (0.09976) COF values were reported at 100 N and 300 N load, respectively, for composition 3. For composition 4, the value of COF first increased up to 150 N load and the reported maximum COF value (0.1608) then started to decrease, and the minimum value (0.0831) was reported at 250 N load as shown in Figure 12(e). For the final composition, i.e., composition 5, the COF first increased up to 150 N load and a maximum COF (0.1586) was reported, which then started to decrease, and a minimum COF of 0.1024 at 300 N load was reported, as shown in Figure 12(f).

Wear volume after the tribological test was calculated using a 3D profilometer (Rtech, USA), and the wear coefficient was calculated by using equation (4) given above. Wear volume and wear rate for all specimens at different loads are shown in Figures 13 and 14 respectively. For base composition, the wear volume linearly increased with an increase in the normal applied load. Maximum (0.6537301 mm^3) and minimum (0.3144331 mm^3) wear volume were reported at normal load 300 N and 100 N, respectively. The wear rate/coefficient for the base composition gradually decreased with an increase in the normal applied load. The maximum (1.69248E-04 mm^3/Nm) and minimum (1.81592E-05 mm^3/Nm) values of wear coefficient were obtained at the normal applied load of 50 N and 300 N load, respectively. Composition 1 showed a similar trend as the base composition for wear volume, but the wear volume

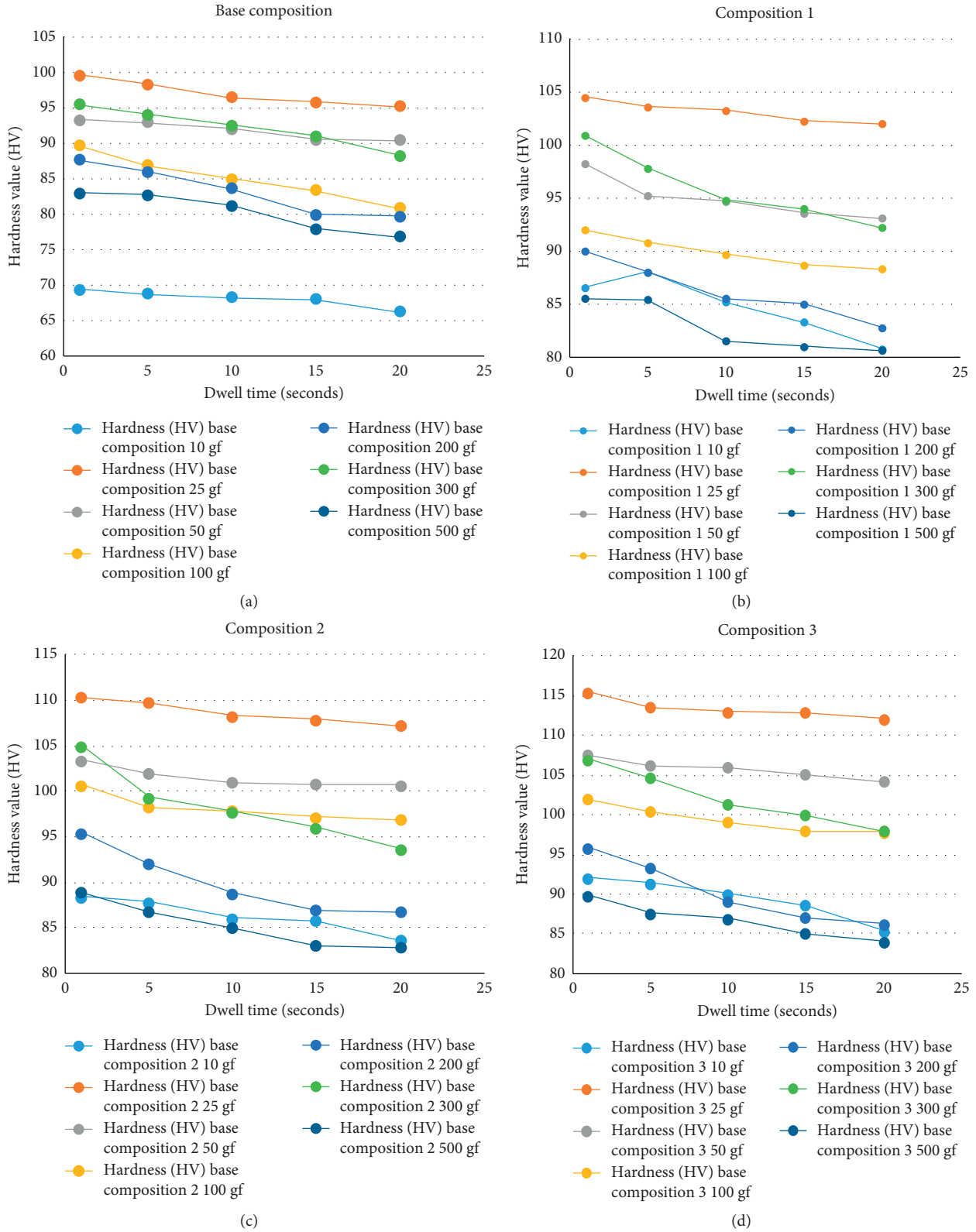

Figure 11: Continued.

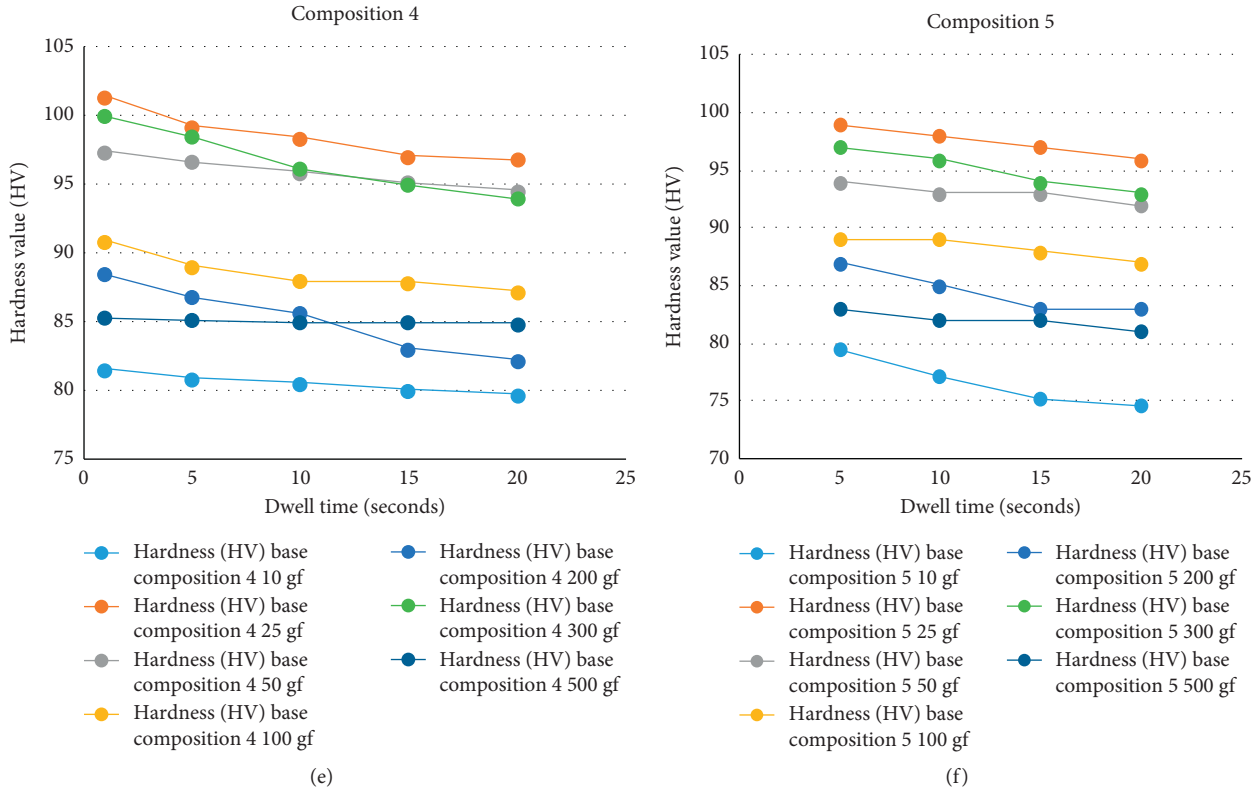

Figure 11: Hardness value versus dwell time graph for different composition samples.

removal was comparatively much lower than that of the base composition. This is due to the introduction of hard phase ceramic reinforcement in the base composition matrix. Minimum (0.3099561 mm^3) and maximum (0.4188146 mm^3) wear volume values were reported at 100 N and 300 N load, respectively. The wear coefficient for composition 1 showed a linearly decreasing trend in terms of wear rate with an increasing applied load. Maximum (8.90999E-05 mm^3/Nm) and minimum (1.23566E-05 mm^3/Nm) wear coefficient values were obtained for 50 N and 250 N normal applied load, respectively.

The wear volume for composition 2 first increased up to 200 N load and then started to decrease. Minimum (0.2685194 mm^3) and maximum (0.3447975 mm^3) wear volume values were reported for 300 N and 200 N load, respectively. The wear coefficient (2.50026E-05 mm^3/Nm) maximum and (7.45887E-06 mm^3/Nm) minimum values were reported at 100 N and 300 N load, respectively. Composition 3 shows the minimum wear volume of 0.2475867 mm^3 at 300 N and maximum wear volume of 0.30862252 mm^3 at 150 N load. Maximum wear coefficient (2.26872E-05 mm^3/Nm) was reported at 100 N and minimum value (6.87741E-06 mm^3/Nm) was reported at 300 N load for composition 3. Compositions 4 and 5 show a similar trend with a linear decrease in the wear volume as the normal load increases. Maximum (0.2981472 mm^3) and minimum (0.25046842 mm^3) wear volume values were reported for composition 4 at 100 N and 300 N load, respectively. In case of composition 5, maximum (0.2956381 mm^3) and minimum (0.232107 mm^3) wear volume values were obtained at 100 N and 300 N load, respectively. For wear coefficient, composition 4 offered a minimum value (6.95746E-06 mm^3/Nm) and maximum value (2.48456E-05 mm^3/Nm) at 300 N and 100 N load, respectively. In case of composition 5, maximum wear coefficient (2.46365E-05 mm^3/Nm) was reported at 100 N, whereas minimum wear coefficient (6.44742E-06 mm^3/Nm) was reported at 300 N normal applied load. From the results, an increase in the reinforcement concentration reduces the wear volume significantly.

4.3. Wear Analysis. Typical modes of wear and damage of material are scoring (abrasion), scuffing (adhesion and diffusion), pitting (fatigue and external attack), and mild wear (delamination and oxidation). These wear types mainly report the appearance aspect of the worn and damaged component. Wear behavior of the material in the early phase is different from the wear behavior after enough sliding. After adequate sliding of the tribo-pair, factors such as surface roughness, COF, magnitude of friction fluctuation, composition, and microstructure control the wear of the material. For wear of the material, many theories have been proposed till now. According to one theory, the wear of the material is because of the loss of the hardness of a metal with contacting surface temperature rise. Another theory proposed that due to the rise in temperature, a sliding surface becomes oxidized and some external force peels off these oxide layers, leading to the wear of the material. The third theory proposed that oxides that are peeled off act as abrasive

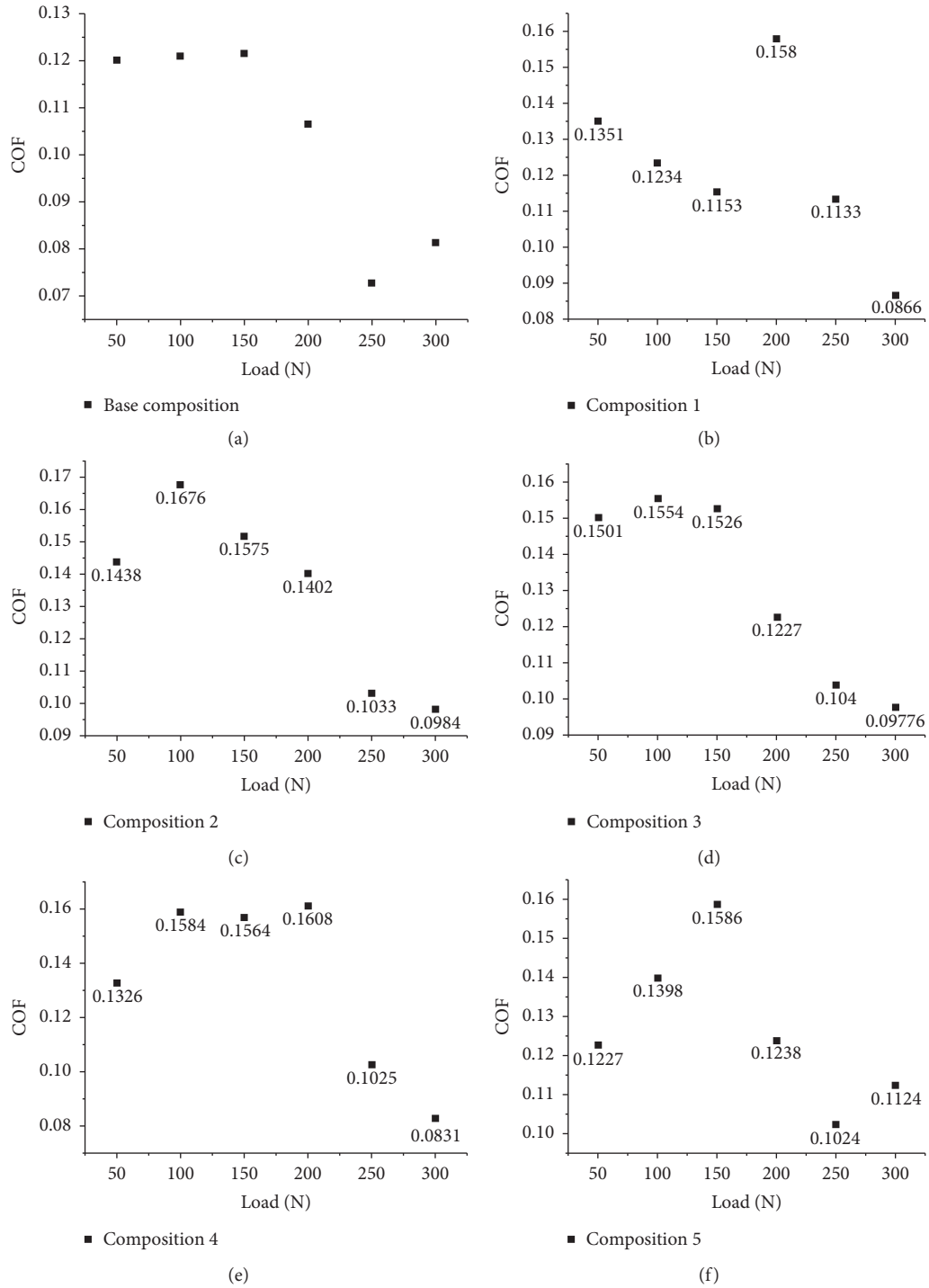

Figure 12: COF v/s load graph for different composite samples. (a) Base composition. (b) Composition 1. (c) Composition 2. (d) Composition 3. (e) Composition 4. (f) Composition 5.

particles which cause abrasive wear in the material. Another mechanism states that by a collective set of micro- and nano-events such as plastic deformation, localized heating leads to wear in the material, but these mechanisms are valid for a range of load and temperature. Srivyas and Charoo [15] reported that the wear of a material is due to ductile and brittle fracture, low and high cyclic fatigue, corrosion, etc.

Optical micrographs (Figure 15) are used for the analysis of the worn-out surface. Under high loading conditions, abrasion, plastic deformation, and oxidation wear were detected. The above stated wear mechanism may lead to the

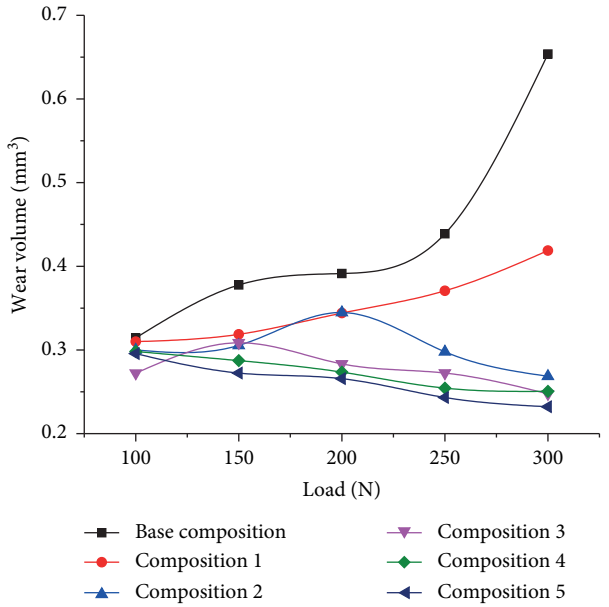

Figure 13: Wear volume v/s load at variable load.

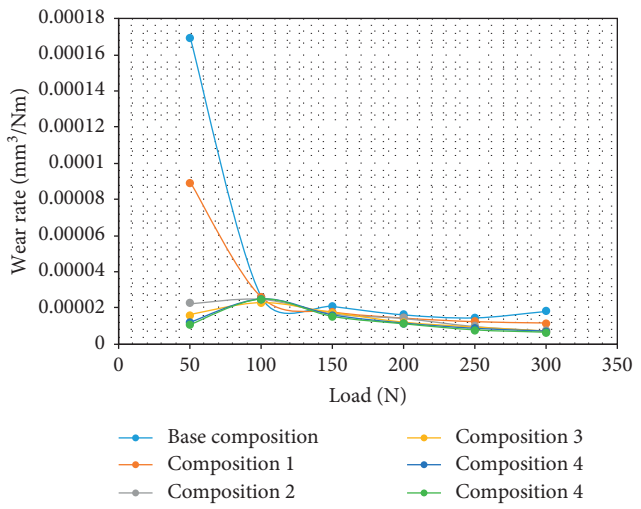

Figure 14: Wear rate v/s load at variable load.

formation of a work-hardened layer, which affects the wear behavior at high load. Wear cracks were also formed on the scar zone which are normal to the direction of sliding, which provides the evidence of delamination wear. A micrograph of the counter-body shows that the transfer of material leads to the adhesion of the counter-body. It is also observed that wear debris particles reattach to the counter-body. Small fragments of oxide particles and silicon particles present on the wear surface act as solid lubricant and cause roller bearing mechanism, influencing the wear of the material. These small particles that were carried out at high load also smoothens the wear tracks. Work hardening of the material surface at high load is because of the plastic deformation. Abrasion wear was observed because of the hard asperities of the counter-body. Deep abrasion marks were observed on the wear scar of the alloy sample. A strong mechanical layer was observed due to the formation of a tribo-layer at the interface, which continuously decreases the wear rate. The same trends were observed at 300 N load for dry sliding. Mild to severe wear transition takes place as the load increases. At a higher load of 300 N, scuffing and seizure wear was reported. Melt wear was also observed at high load of 200–300 N. A melt layer was reported, which prevents further removal of the material. Localized melt at high load takes place due to the rise in contact surface temperature.

SEM (Figure 16) studies show abrasion and deep grooves on the wear scar. EDS analysis confirms the presence of Si particles on the wear scar, and it is observed that the material adheres on the steel ball. Abrasion wear is responsible for the loss of material and indicates that metallic wear is due to abrasion. Increased contamination of the oxide layer was reported for the alumina-reinforced composite sample. The presence of this oxide reduces direct metal-metal contact and, hence, prevents asperity-asperity contact in the case of the composite sample. SEM micrographs revealed the presence of abrasion marks, cracks, work-hardened layer of oxides, and tribo-layer formation on the wear scar zone. The EDS analysis confirmed the transfer of material and oxide layer formation. The SEM micrograph shows severe abrasion, plastic deformation, and oxidation as the main wear mechanism at high load for the fabricated samples.

3D profilometer image, roughness profile, and texture of the wear scar are shown in Figure 17. These studies were made to analyze the effect of the tribological test on the wear scar profile. For base composition, where no protective layer was formed, the roughness of the wear scar was found to be high. For base composition, the roughness value (Ra) at 50 N load was 12.9 μm; a further increase in the applied load lead to an increase in the roughness of the contacting scar surface, creating a wider wear scar width and less depth scar texture profile. For load 100 N, 200 N, and 300 N, the roughness value was obtained to be 13.5 μm, 17.3 μm, and 24.2 μm, respectively. From the previous studies, it was reported that the wear scar width does not increase if the post-testing surface is not smooth, i.e., has a high roughness value; similar is the case with scar depth. It was also reported that during the run-in period, there is an asperity-asperity contact, which has an impact on the friction behavior. So, it is clear from the fact that the initial roughness of the contacting surface affects the friction properties of the material. For composition 1, (Ra) roughness values of 7.1 μm, 4.5 μm, 4.79 μm, and 5.1 μm for 50 N, 100 N, 200 N, and 300 N load, respectively, were reported. Further for composition 2, roughness values of 6.02 μm, 4.82 μm, 4.54 μm, and 4.07 μm were reported for 50 N, 100 N, 200 N, and 300 N load, respectively. For the composite sample, the roughness value and texture profile were studied. It was reported that the increase in the reinforcement leads to a decrease in the wear scar width texture and depth of the wear scar. For composition 3, the Ra values at 50 N, 100 N, 200 N, and 300 N were observed to be 6.13 μm, 3.76 μm, 4.33 μm, and 4.42 μm, respectively. Composition 5 shows a minimum

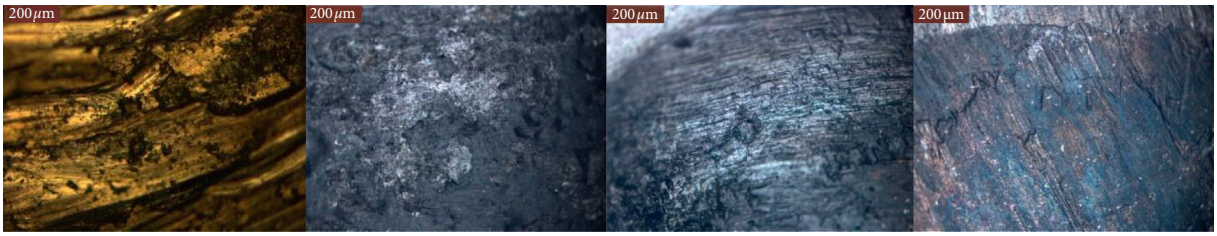

(a)

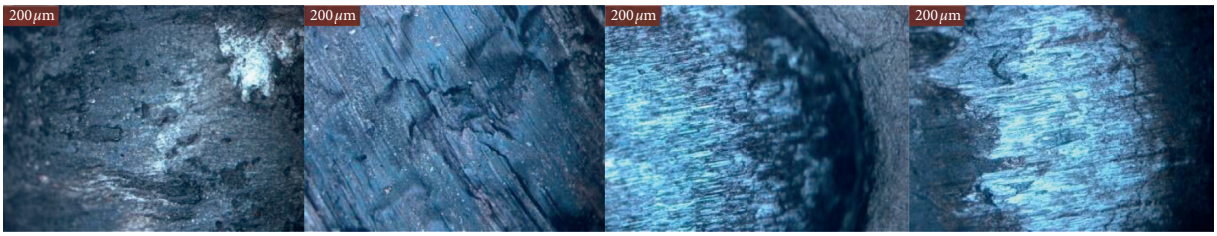

(b)

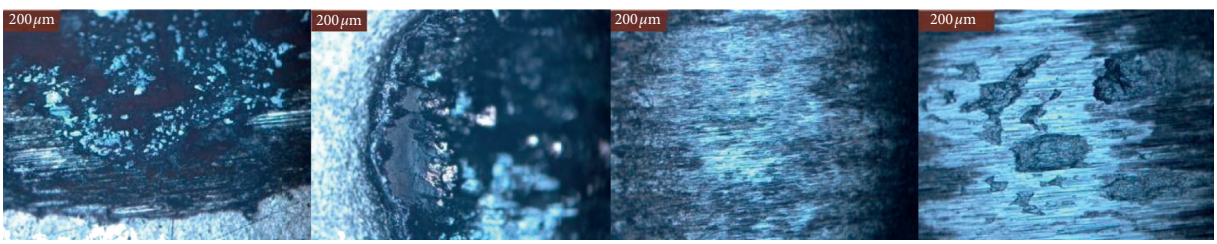

(c)

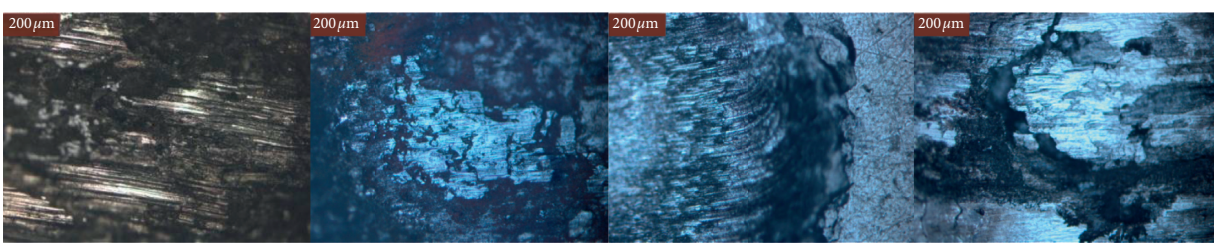

(d)

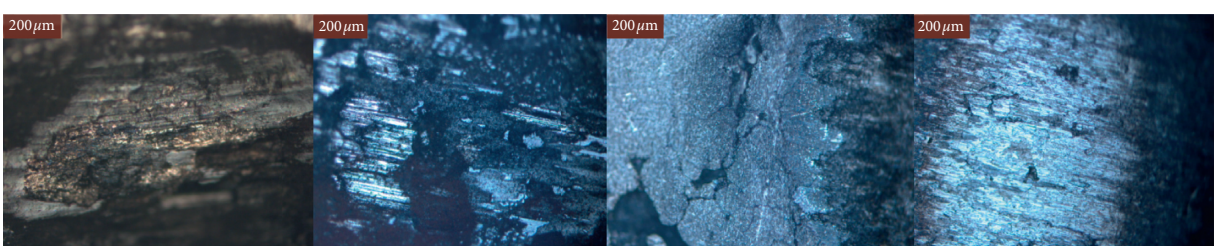

(e)

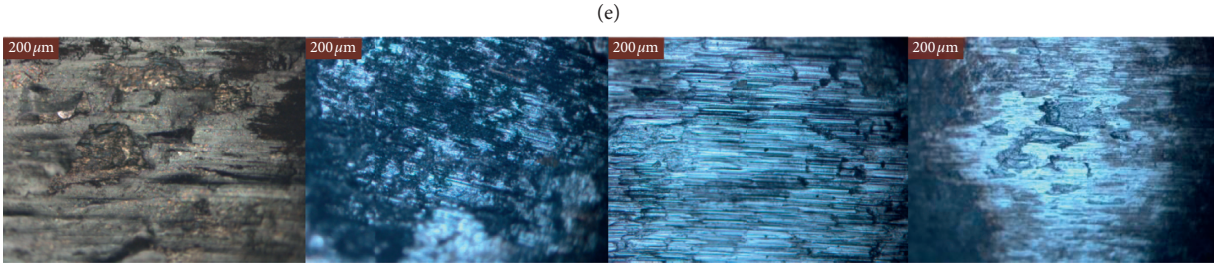

(f)

Figure 15: Continued.

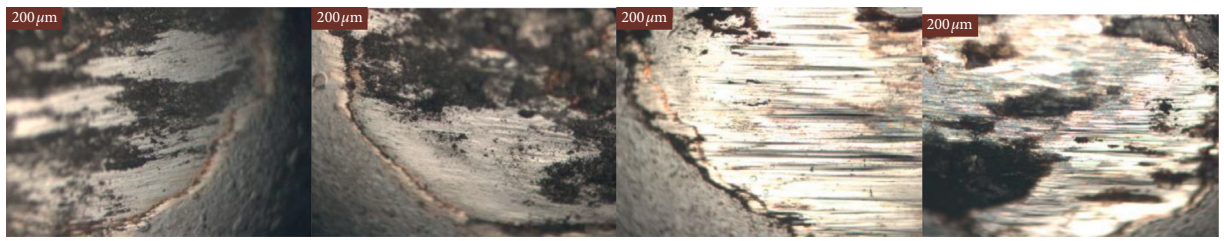

(g)

Figure 15: Optical micrographs of the composite samples and counter-body. (a) Base composition. (b) Composition 1. (c) Composition 2. (d) Composition 3. (e) Composition 4. (f) Composition 5. (g) Counter-body.

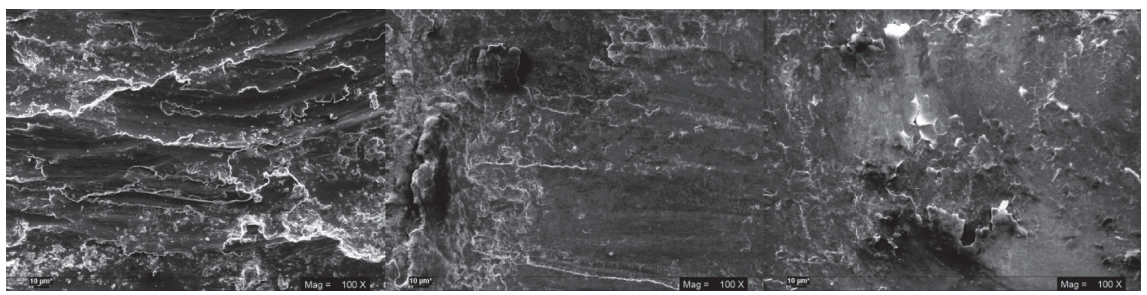

(a)

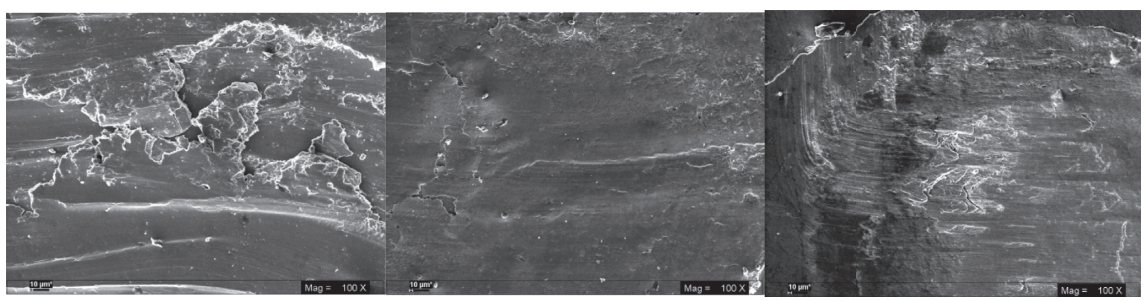

(b)

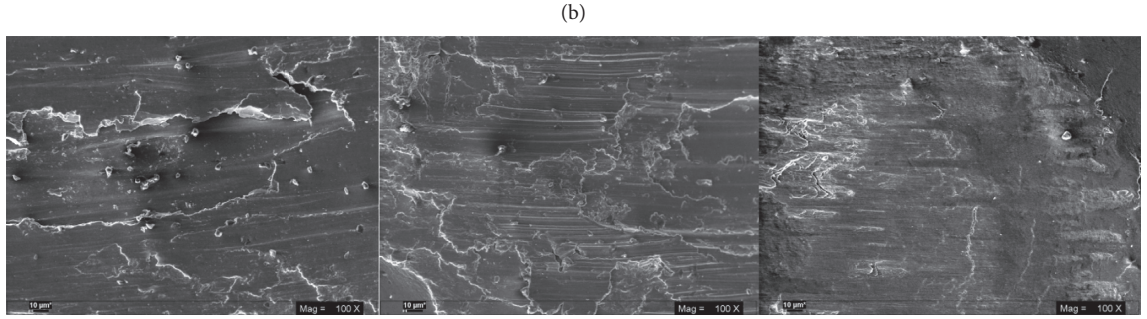

(c)

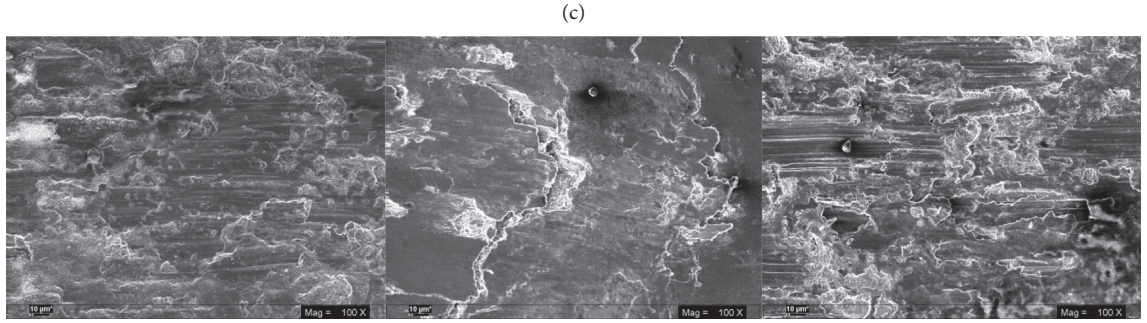

(d)

Figure 16: Continued.

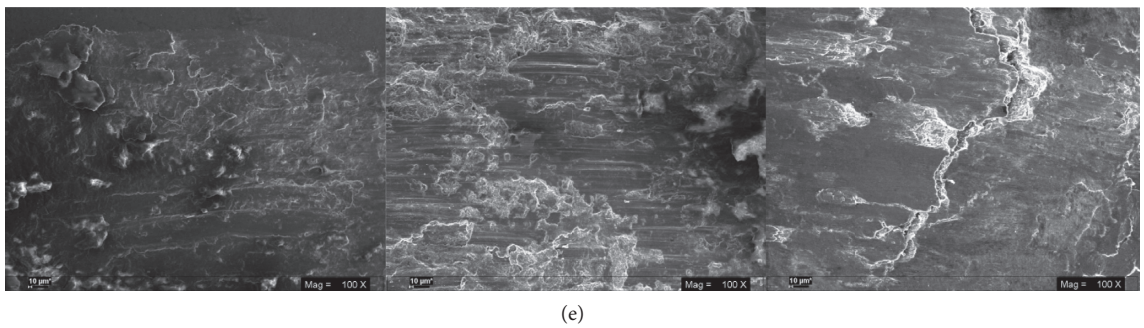

(e)

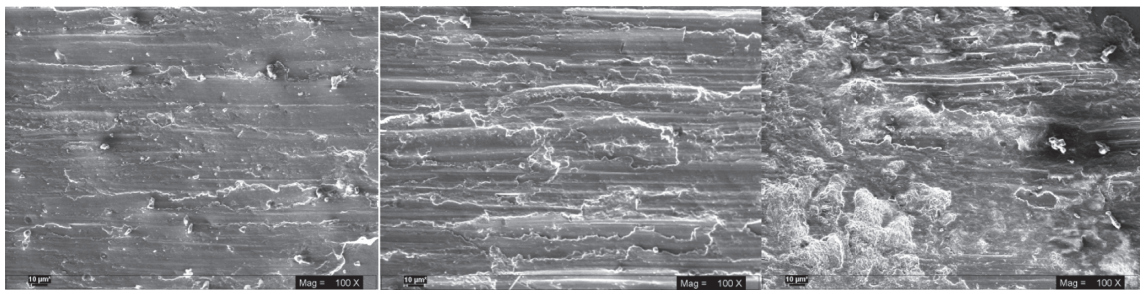

(f)

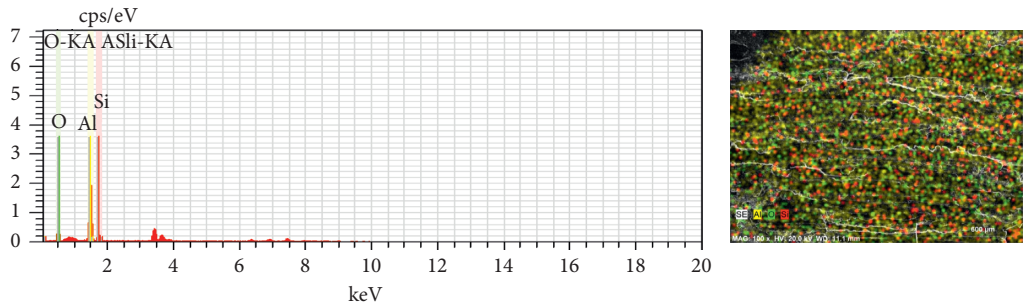

(g)

Figure 16: Wear scar observed under SEM and EDS analyses. (a) Base composition. (b) Composition 1. (c) Composition 2. (d) Composition 3. (e) Composition 4. (f) Composition 5.

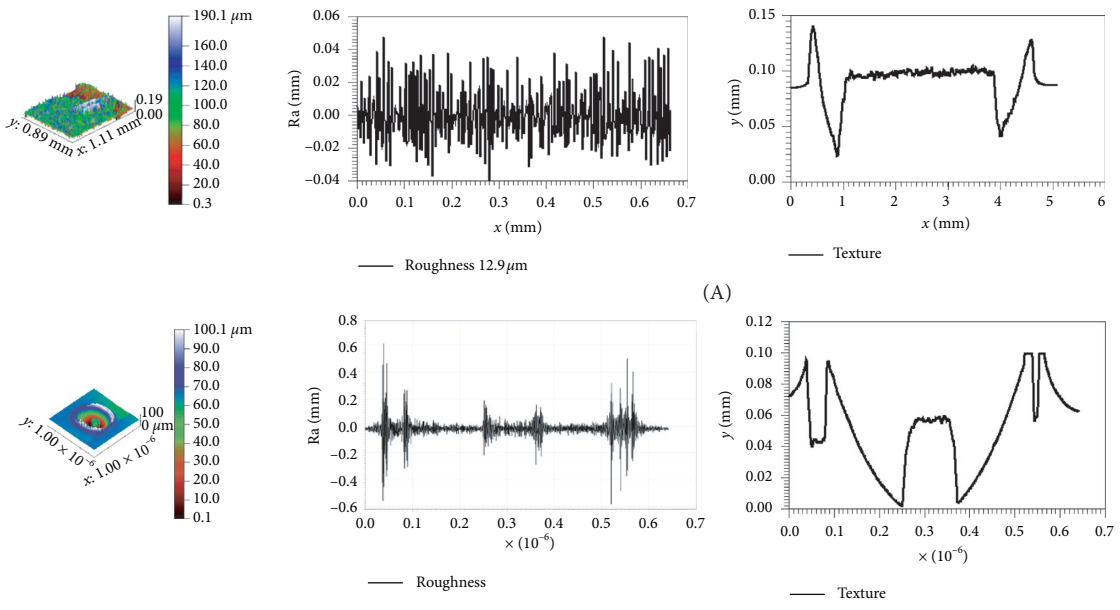

(a)

Figure 17: Continued.

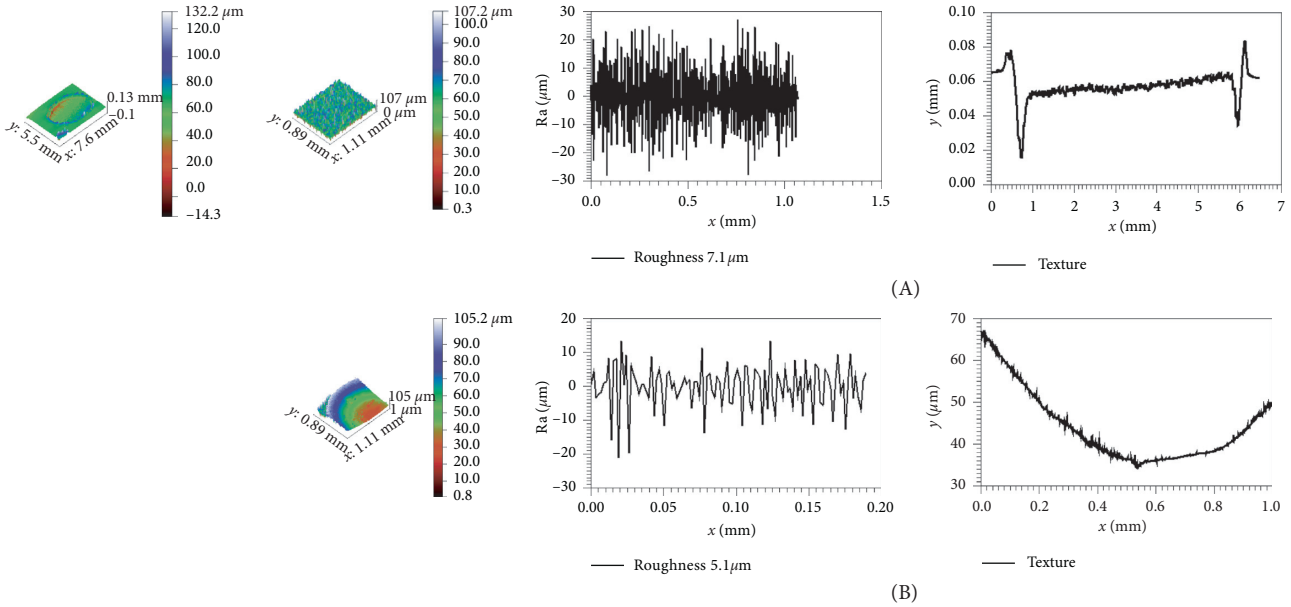

Figure 17: Continued.

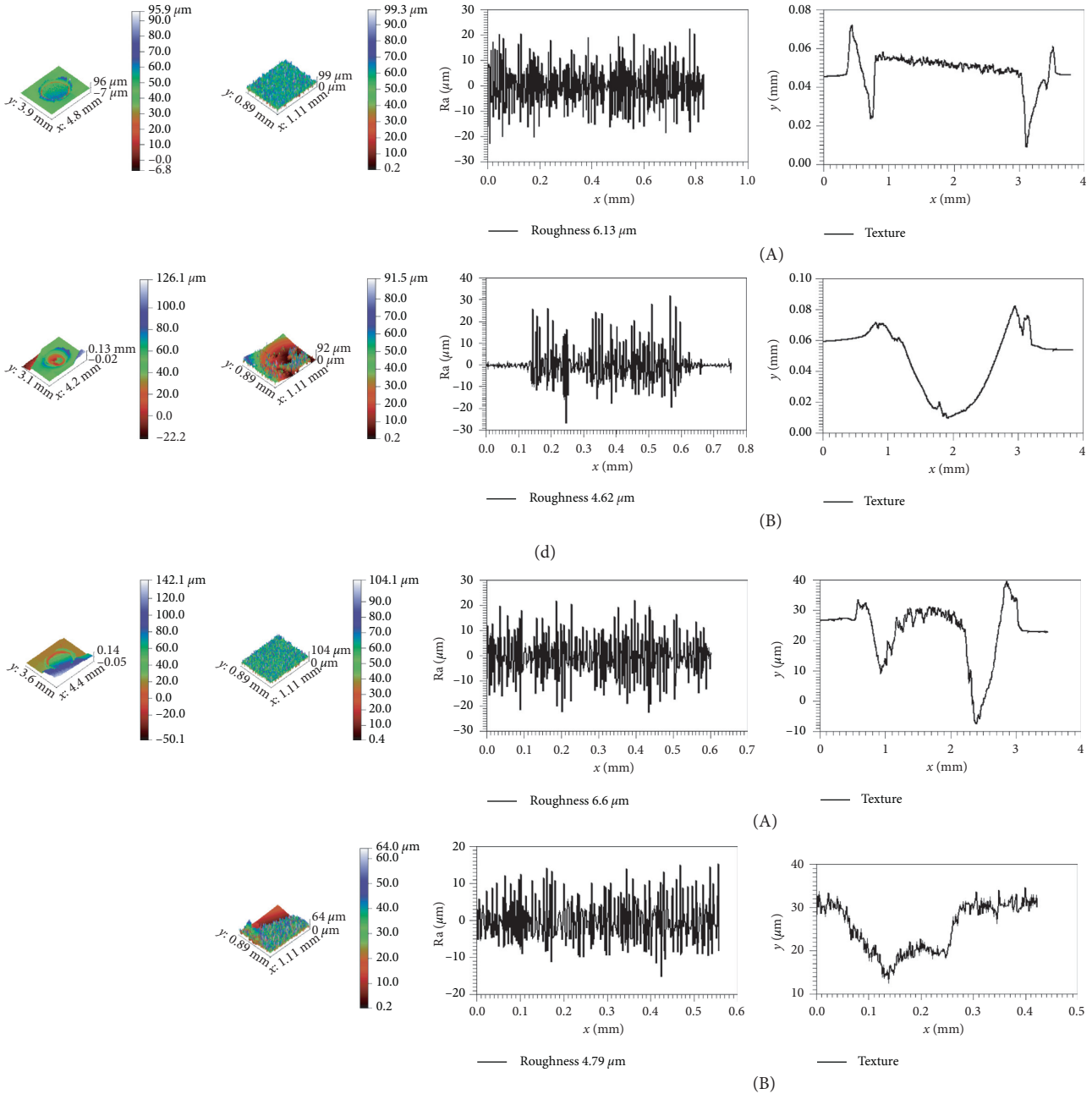

Figure 17: Continued.

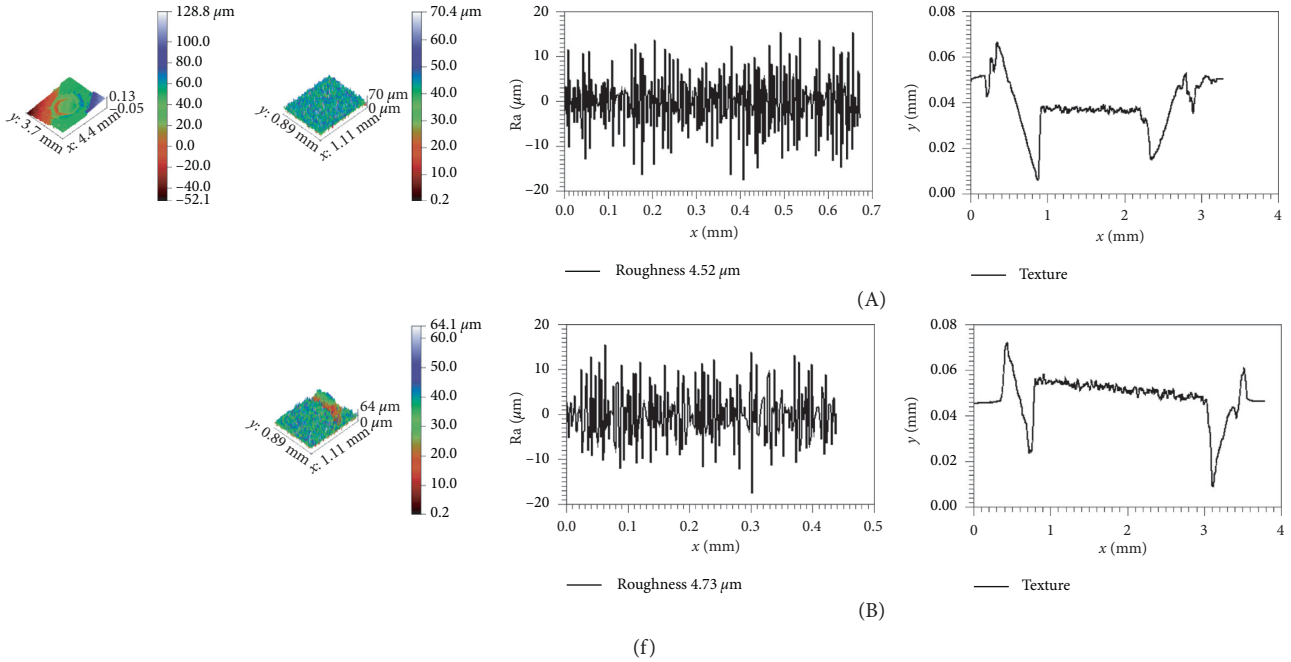

FIGURE 17: 3D profilometer image, roughness profile, and texture analysis of the wear scar ((A) 50 N load and (B) 300 N load). (a) Base composition. (b) Composition 1. (c) Composition 2. (d) Composition 3. (e) Composition 4. (f) Composition 5.

value for roughness (Ra) of 4.52 μm at 50 N load. Reduction in the wear scar roughness was observed, which is due to the formation of a smooth tribo-film on the wear scar.

5. Conclusion

This work aimed to investigate the influence of load on the tribological properties of Al-Si eutectic reinforced n-Al_2O_3 under dry sliding conditions. Its main objective was to provide a new contribution to the tribological behavior of these composites fabricated using the nonconventional spark plasma sintering method. On the basis of the results obtained from the experimentation, the following can be concluded:

(1) Fabrication of Al-Si/Al_2O_3 nanocomposites using a high-energy ball mill, followed by the nonconventional spark plasma sintering method, results in highly dense (near theoretical), low porosity samples with better mechanical and tribological properties.

(2) Microhardness studies were done on the nanocomposite samples, and these nanocomposites exhibited higher hardness, which is because of the proper/homogeneous dispersion of the reinforcement in the matrix material. It is also attributed to the introduction of hard phase reinforcement in the matrix material.

(3) Tribological studies were performed at high load (50 N–300 N). Reduction in wear volume for the advanced composite was reported in the range 15.45–44.58% compared to the base alloy (eutectic Al-Si alloy). An increase in the friction coefficient was reported in the range 28.80–35.65% compared to the base matrix alloy material. It was observed that the wear volume of the composite material decreases with an increase in the reinforcement content.

(4) The increase in the surface roughness of the fabricated material due to relative sliding decreases by 44.96–64.96% compared to the base matrix alloy. It is also reported that with the increase in the load, the roughness value decreases. It was attributed to the enormous pressure on the contacting surface, which crushes and fractures the asperities.

(5) This reduction in wear volume is attributed to the introduction of hard phase reinforcement in the matrix material. Abrasion, plastic deformation, work-hardened layers, and cracks on the interface were the main wear mechanism at high loading tribo testing conditions.

Data Availability

The data used to support the findings of this study are included within the article text. Previously reported data were used to support the current research study. Prior studies are cited at the relevant places within the text as references.

Conflicts of Interest

The authors declare that there are no conflicts of interest regarding the publication of this paper.

Acknowledgments

The authors gratefully acknowledge all the researchers who have worked in the field of tribology; without their

significant contribution, this experimental study would have been difficult to summarize. The authors also want to acknowledge their institute and supervisor for their wholehearted support.

References

[1] A. Anand and M. F. Wani, "Product life-cycle modeling and evaluation at the conceptual design stage: a digraph and matrix approach," *Journal of Mechanical Design*, vol. 132, no. 9, p. 9, 2010.

[2] J. Hirsch, "Recent development in aluminium for automotive applications," *Transactions of Nonferrous Metals Society of China*, vol. 24, no. 7, pp. 1995–2002, 2014.

[3] W. S. Miller, L. Zhuang, J. Bottema et al., "Recent development in aluminium alloys for the automotive industry," *Materials Science and Engineering: A*, vol. 280, no. 1, pp. 37–49, 2000.

[4] R. Molina, P. Amalberto, and M. Rosso, "Mechanical characterization of aluminium alloys for high temperature applications Part1: Al-Si-Cu alloys," *Metallurgical Science and Tecnology*, vol. 29, 2011.

[5] P. Rambabu, N. Eswara Prasad, V. V. Kutumbarao, and R. J. H. Wanhill, "Aluminium alloys for aerospace applications," *Aerospace Materials and Material Technologies*, pp. 29–52, 2017.

[6] R. Ahmad and M. B. A. Asmael, "Influence of lanthanum on solidification, microstructure, and mechanical properties of eutectic Al-Si piston alloy," *Journal of Materials Engineering and Performance*, vol. 25, no. 7, pp. 2799–2813, 2016.

[7] S. Milenkovic, V. Dalbert, R. Marinkovic, and A. W. Hassel, "Selective matrix dissolution in an Al-Si eutectic," *Corrosion Science*, vol. 51, no. 7, pp. 1490–1495, 2009.

[8] R. Shivanath, P. K. Sengupta, and T. S. Eyre, "Wear of aluminum-silicon alloys," in *Proceedings of International Conference of Wear of Materials 1977*, pp. 120–126, ASME, New York, NY, USA, April 1977.

[9] B. N. P. Bai and S. K. Biswas, "Characterization of dry sliding wear of Al Si alloys," *Wear*, vol. 120, no. 1, pp. 61–74, 1987.

[10] T. S. Eyre, "Wear of aluminium alloys," *Microstruct Sci*, vol. 8, pp. 141–151, 1980.

[11] A. J. Clegg and A. A. Das, "Wear of a hypereutectic aluminium-silicon alloy," *Wear*, vol. 43, no. 3, pp. 367–373, 1977.

[12] G. Rajaram, S. Kumaran, and T. S. Rao, "High temperature tensile and wear behaviour of aluminum silicon alloy," *Materials Science and Engineering: A*, vol. 528, no. 1, pp. 247–253, 2010.

[13] M. Dhiman, D. K. Dwivedi, R. Sehgal, and I. Bhat, "Effect of iron on wear behavior of as-cast and heat-treated hypereutectic Al-18Si-4Cu-0.5Mg alloy: a Taguchi approach," *Proceedings of the Institution of Mechanical Engineers, Part L: Journal of Materials: Design and Applications*, vol. 228, no. 1, pp. 2–16, 2014.

[14] A. K. Dahle, K. Nogita, S. D. McDonald, C. Dinnis, and L. Lu, "Eutectic modification and microstructure development in Al-Si alloys," *Materials Science and Engineering: A*, vol. 413-414, pp. 243–248, 2005.

[15] P. D. Srivyas and M. S. Charoo, "Effect of load on the tribological behavior of self-lubricating hybrid aluminum composite under dry sliding conditions," *Materials Research Express*, vol. 6, no. 12, p. 125702, 2019.